1. Grzegorz KŁOSOWSKI[2], 2. Przemysław ADAMKIEWICZ [1], 3. Jan SIKORA[1,2]

University of Economics and Innovation in Lublin (1), Research and Development Center Netrix S.A. (2),
Lublin University of Technology (3)
1.   0000-0001-7927-3674, 2. 0000-0003-3425-9566, 3. 0000-0002-9492-5818
2.

The use of convolutional neural networks in radio tomographic imaging

Abstract. This work aims to solve the problem of tracking people's movement in closed spaces. The applied solution does not require the monitored persons to have any devices with them. The method presented is to use radio tomographic imaging based on the fact that the human body is mostly water. This paper aims to show how heterogeneous and convolutional neural networks can be used to improve a radio tomographic imaging system that can accurately locate people indoors. In addition to the original algorithmic solutions, the advantages of the system include the use of properly designed and integrated devices - radio probes - whose task is to emit Wi-Fi waves and measure the strength of the received signal. Thanks to the two-step approach, the sensitivity, resolution and accuracy of imaging have increased. In addition, our solution performs well in radio tomography and other types of tomography because it is easy to understand and can be used in many ways.

*Streszczenie. Niniejsza praca ma na celu rozwiązanie problemu śledzenia ruchu osób w pomieszczaniach zamkniętych. Zastosowane rozwiązanie nie wymaga, aby monitorowane osoby posiadały przy sobie jakiekolwiek urządzenia. Przedstawiony sposób polega na wykorzystaniu tomograficznego obrazowania radiowego w oparciu o fakt, że ciało ludzkie składa się w większości z wody. Niniejsze opracowanie ma na celu pokazanie, w jaki sposób niejednorodne, splotowe sieci neuronowe można wykorzystać do ulepszenia systemu obrazowania radiotomograficznego, który może precyzyjnie znajdować ludzi w pomieszczeniach. Oprócz oryginalnych rozwiązań algorytmicznych do zalet systemu należy zastosowanie odpowiednio zaprojektowanych i zintegrowanych urządzeń – sond radiowych – których zadaniem jest emitowanie fal Wi-Fi oraz pomiar siły odbieranego sygnału. Dzięki zastosowaniu podejścia dwuetapowego wzrosła czułość, rozdzielczość i dokładność obrazowania. Ponadto nasze rozwiązanie dobrze sprawdza się w tomografii radiowej i innych rodzajach tomografii, ponieważ jest łatwe do zrozumienia i może być używane na wiele sposobów. (**Wykorzystanie konwolucyjnych sieci neuronowych w obrazowaniu radiotomograficznym**).*

Keywords: radio tomographic imaging, device-free localization, artificial neural networks, wireless localization
Słowa kluczowe: tomografia radiowa; lokalizacja bez urządzeń; sztuczne sieci neuronowe, lokalizacja bezprzewodowa

Introduction

Along with the development of megatrends related to the integration of high technologies with the changing standards of the functioning of businesses and societies, there is a growing need to develop mechanisms for monitoring people in closed spaces. In the case of shopping centres, airports, stations, museums, market halls, etc., the main goal is to ensure the safety and comfort of customers and to optimize the movement of people. On the other hand, in the case of buildings with restricted access, such as prisons, military facilities, hospitals, office buildings, production halls, industrial installations, etc., the aim is to monitor people in order to restrict access to specific rooms and eliminate threats, e.g., terrorist threats.

The development of intelligent building technologies depends on the advancement of many cyber-physical systems, each of which fulfils specific tasks [1]. Intelligent building technologies rely on many cyber-physical systems, each of which does a different aim. Radio tomographic imaging (RTI) makes it possible to localize and track people without them having to carry any extra electronic devices [2–5]. Effective implementation of such a solution enables constant monitoring of the location of people in buildings for various purposes, such as production halls, shopping centers, sports stadiums, closed facilities (e.g., prisons), amusement parks, hospitals, museums, etc. An important advantage of the RTI system is the relatively low cost of implementation and maintenance [6]. Such information can be used to automate human-responsive intelligent building subsystems such as lighting, air conditioning, heating, door locking control, shutter control, etc., as well as for security purposes. Device-free locating people inside buildings is a challenge due to the difficulties associated with the need to solve the tomographic inverse problem. This problem is also ill-posed, which results from the deficit of the explanatory variables in relation to the dependent variables [7-13]. Due to the above difficulties, currently known methods still require improvement in the quality of algorithms for converting RT measurements to images.

The popularity of free machine learning libraries has spurred interest in improving machine learning algorithms in RTI systems. In [1], the authors attempt to mathematically design estimators to reduce the uncertainty resulting from the quantization error of received signal strength (RSS) that makes up the output data. In [4], the authors present the RTI reconstruction through the Landweber iteration process with one-step multiplication. To solve the ill-posedness problem, they use Tikhonov regularization. Another example of research on the wireless location of people using a network of sensors is the study [14]. In this case, researchers prove that shadow fading can be represented as a linear combination of the proportion of radio frequency (RF) links. This transformation, called back projection, indicates that the selection of RF information links contributes to the reduction of measurement noise. The image reconstruction is created using a technique that is based on Bayesian Compressive Sensing and back projection. Other ways to improve the quality of RTI imaging include using hybrid grids to make images, interference cancelling techniques, heterogeneous Bayesian compressive sensing [15], generative model-based attenuation image recovery [16], and others.

The main objective of this paper is to present a concept of the algorithmic method that significantly contributes to the improvement of RTI images. RTI development typically focuses on single issues related to mathematical modelling, inverse problem algorithms, or hardware solutions. Our method improves the performance of two tasks simultaneously (image creation and postprocessing), and its additional advantage is its versatility, which makes it applicable not only to RTI but also to other types of tomography, such as electrical or ultrasound tomography.

Materials and Methods

An important element of the research is the correct design of the matrix on which the tomographic image will be created. A mathematical model of the Fresnel zone was used for this purpose. The Fresnel zone is an ellipse-shaped space that is correlated with the transmission energy of the radio signal between a transmitter and a receiver. The longitudinal section of the Fresnel zone is elliptical in shape, as can be seen in Figure 1, which presents the RF network consisting of 16 sensors with an illustration of the weight model. Each of the 16 sensors (nodes) can transmit and receive a WiFi signal by connecting to any other node. In this way, we obtain a network of 120 two-way connections.
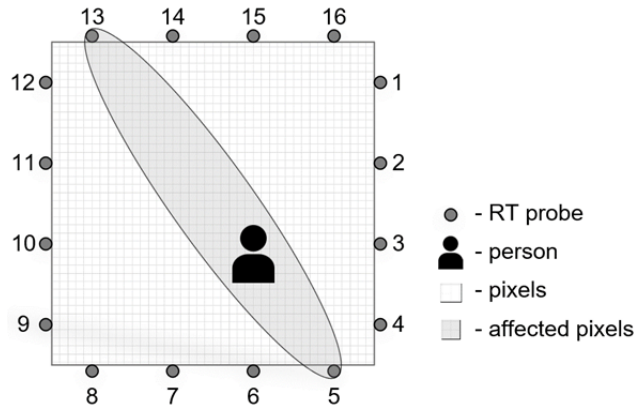
Fig. 1. RF sensor network with elliptical weight model

We can put a pixel mesh on the analyzed surface. Measurable radio signals between the transmitter and receiver propagate inside a rotating ellipse called the first Freshnel zone. Thus, an object (e.g., a human) that is located in the area of the ellipse weakens the received radio signal. On this basis, the weights of pixels that are inside the ellipse w_{ij} can be determined according to formula (1)

$$(1) \qquad w_{ij} = \frac{1}{\sqrt{d_i}} \begin{cases} 1 & if \quad d_{ij}^1 - d_{ij}^2 < d_i + \delta \\ 0 & else \end{cases}$$

where d_i represents the distance between the pair of WiFi sensors, d_{ij}^1 and d_{ij}^2 are the distances from the center of the pixel i to the sensor locations j, δ is the adjustable parameter that determines the width of the ellipse. External pixels are assigned zero weights ($w_{ij} = 0$). Formula (1) can be presented in the generalized matrix form $\mathbf{y} = \mathbf{w}\mathbf{x} + \mathbf{n}$, where $\mathbf{y}$, $\mathbf{x}$, and $\mathbf{n}$ are the shadowing, pixels, and noise vectors respectively, $\mathbf{w}$ is the matrix of weights. Figure 2 shows a room with probes placed on the walls.

Fig. 2. (a) – the room with WiFi probes installed on the walls, (b) – a close-up of the probes with USB power supply

The WiFi radio transducer consists of a microcontroller with an ARM architecture, a radio wave transmitter compatible with Bluetooth 5, and a transmitter using the IEEE 802.15.4 transmission standard. The above elements were enclosed in a module the size of a matchbox. The transmitters use the 2.4 GHz band and the same modulation (GFSK) but with the division into other channels characteristic of their protocols. The efficiency of data exchange is favored by the use of two independent antenna paths, one of which was made as a ceramic antenna integrated with the PCB, and the other as an external antenna for the u.FL connector. Figure 3 shows the WiFi transducer integrated circuit.
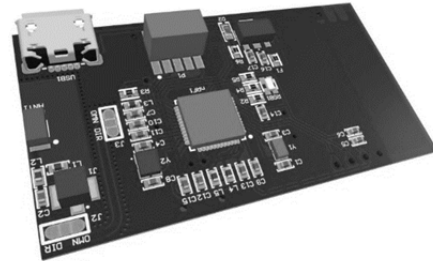

Fig. 3. WiFi transducer integrated circuit

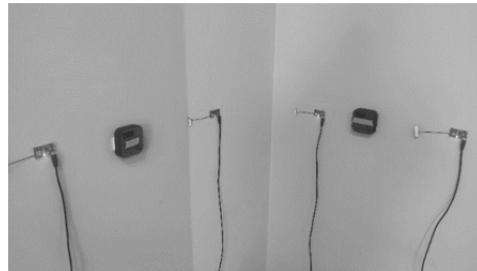Figure 4 presents the room with WiFi probes installed on the walls with USB power supply.

Fig. 4. The WiFi transducers mounted on the walls.

In Figure 5a, we can see the outline of the room marked with the places of installation of sixteen WiFi probes. In turn, Figure 5b shows the pattern of a case reflecting three tracked objects located in the observed room.
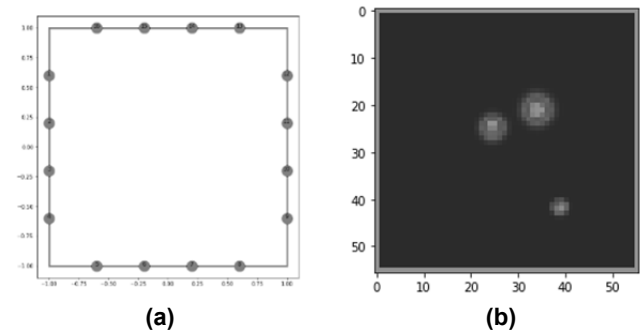

Fig. 5. Monitored room: (a) - a room with transducers, (b) – pattern image with tracked objects.

Figure 6 shows reconstruction images with a resolution of 56×56 pixels. As you can see, the quality of both reconstructions, both raw and filtered, is very poor.

As an alternative method, we propose the use of two convolutional neural networks (CNN), the first of which CNN_1 is designed to reconstruct images based on measurements. Since the CNN_1 network solves the inverse problem, the resulting reconstructions are not perfect. To improve the quality of the reconstruction, we train the second CNN_2 network. Using a trained CNN_1 network, we

generate reconstructions that will be used as inputs during the training of the second CNN_2 neural network. The two-stage workflow of this concept is presented in formula (2)
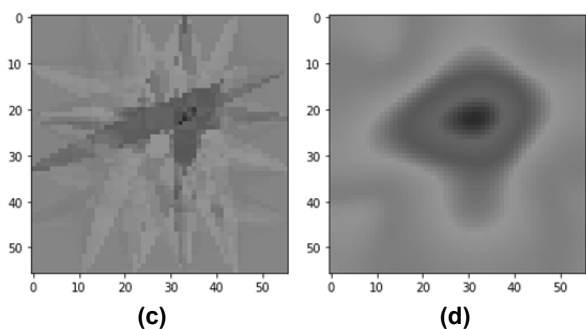

Fig. 6. Mathematically simulated reconstructions: (a) – reconstruction with elliptical weight model, (b) – filtered reconstruction

$$(2) \quad \begin{cases} \mathbf{X} \to CCN_1 \to \widehat{\mathbf{Y}} \\ \widehat{\mathbf{Y}} \to CCN_2 \to \breve{\mathbf{Y}} \end{cases}$$

where $\mathbf{X}$ is the 16×16 matrix of measurements, $\widehat{\mathbf{Y}}$ is the 56×56 matrix of reconstructions made by CCN_1, and $\breve{\mathbf{Y}}$ is the 56×56 image enhanced by CCN_2. The Matlab package was used in the research. CNN_1 consisted of 10 layers, including two convolutional, ReLu, batch normalization, and dropout. To counteract overfitting, the early stopping method and a dropout layer with a coefficient of 0.3 were used. CNN_2 consisted of 9 layers and similarly contained two convolutional layers and one fully connected layer.

Figure 7a shows the conversion of the measurement matrix into a reconstruction image. The above conversion is accomplished by means of a convolutional neural network that transforms the set of measurements generated by the transducers. Clearly, the raw restoration produced by CNN is far from perfect. First of all, the proportions of the size of the inclusions are not properly maintained. In the reference picture, the center inclusion is smaller than the one near the south wall of the room.
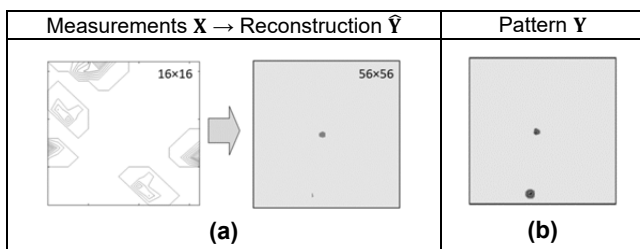

Fig. 7. Producing reconstruction in step 1: (a) – transition from measurements to reconstruction image, (b) – pattern image

Relatively poor quality of reconstructions made on the basis of a single neural network and raw measurement data is understandable because uncorrelated measurement data (120 two-way connections) constitute less than half of all values of the input set (16 × 16 = 256). Meanwhile, the resolution of the reconstruction image is 56 × 56 = 3136 pixels. As it can see, there is a very serious deficit of input data here, which intensifies the scale of the problem of inverse indeterminacy with which the neural network must struggle. For this reason, a second CNN was used to improve the quality of the primary reconstruction (see Figure 8).

The second CNN was trained to use primary reconstructions as inputs and pattern images as outputs. It is clearly visible that after passing the second CNN, the reconstruction image improved, and the proportions of the inclusions became correct.
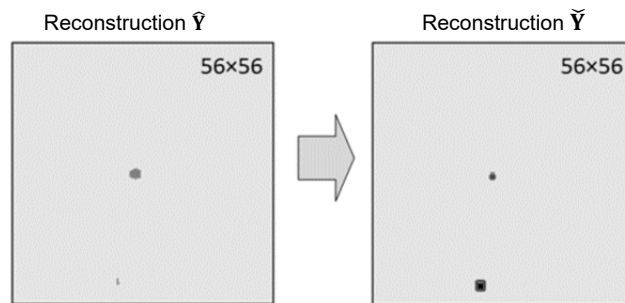

Fig. 8. Improving reconstruction in step 2: (a) – raw reconstruction $\widehat{\mathbf{Y}}$, (b) – enhanced reconstruction $\breve{\mathbf{Y}}$

Results

Fig. 4 shows a comparison of the reconstructions reconstructed by CNN_1 and improved by CNN_2. It can be clearly seen that the reconstructions obtained after using CNN_2 are more accurate and make it possible to locate even small objects located close to each other. This means being able to distinguish between adults and children, or even animals.
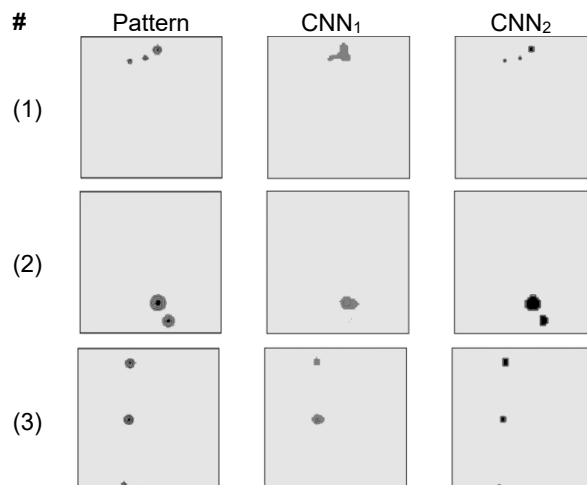

Fig. 9. Comparison of reconstructions reconstructed by CNN1 (1st stage) and improved by CNN2 (2dn stage)

Subjective observations indicate a clear dominance of the reconstructions corrected in the second step, but it is impossible to state this fact indisputably on this basis. The use of quantitative indicators enables an objective evaluation of the reconstructed images in comparison to their standard variants. As many as five independent indicators were used in the research, thanks to which the effectiveness of the described solution was verified. The first and at the same time basic indicator is the mean square error (MSE) [17] calculated according to formula (3)

$$(3) \quad MSE = \frac{\sum_{i=1}^{N}(y_i - \hat{y}_i)^2}{N}$$

where y is a set of pixels included in the pattern image, $\hat{y}$ is a set of pixels included in the reconstruction after the first step. Let's agree that $\breve{y}$ is the analogous set of pixels included in the reconstruction after the second stage. N is the resolution of the image. In this case $N = 3136$.

Another metric is the relative image error (RIE) satisfied by (4).

$$(4) \qquad \text{RIE} = \frac{\|\hat{y} - y\|}{\|y\|}$$

The next indicator is the image correlation coefficient (ICC) expressed by formula (5).

$$(5) \qquad \text{ICC} = \frac{\sum_{i=1}^{N}(y_i - \bar{y})(\hat{y}_i - \bar{\hat{y}})}{\sqrt{\sum_{i=1}^{N}(y_i - \bar{y})^2 \sum_{i=1}^{N}(\hat{y}_i - \bar{\hat{y}})^2}}$$

The sixth criterion for assessing image quality is the mean absolute error (MAE) given by equation (6).

$$(6) \qquad \text{MAE} = \frac{\sum_{i=1}^{N}|(y_i - \hat{y}_i)|}{N}$$

The last indicator is the standard error (SE). The standard error is an estimate of the standard deviation of the difference between the measured (estimated) value and the true value. It can be calculated according to (7)

$$(7) \qquad \text{SE} = \frac{\sigma}{\sqrt{N}}$$

where σ is a standard deviation of absolute error Δy, where $\Delta y = y - \hat{y}$. The true value of the standard error is usually unknown, and the standard deviation of the sample mean distribution is taken as the standard error. Table 1 presents the results of the analysis based on the five above-described criteria for assessing the quality of the reconstructed images. All indicators, except ICC, reflect errors, so the closer their values are to zero, the more the reconstructed image resembles the pattern. ICC is a correlation coefficient, so its maximum value is 1 and its minimum value is zero. The ideal correction of the reconstruction with the pattern would obtain ICC = 1.

Table 1. The parameters of the sensor

Step	MSE	RIE	ICC	MAE	SE
CNN$_1$	0.0012	36.0167	0.7600	1.2441	3.3144
CNN$_2$	0.0008	26.6910	0.8621	0.9433	2.2864

The analysis of the indicators included in Table 1 clearly shows the absolute dominance of the method based on the two-stage process of tomographic imaging.

5 Conclusions

The research conducted experiments aimed at developing neural models and verifying the effectiveness of convolutional neural networks in radio tomography aimed at tracking people in closed spaces. An important feature of the research was testing devices based on inexpensive and popular wireless technologies (WiFi) in relation to people not equipped with any communication devices. This solution is much more flexible and brings real benefits in practical applications.

Convolutional neural networks can solve the inverse problem in RTI. To improve the quality of images, we propose to enter an additional CNN$_2$. We then use CNN$_1$ to generate the training cases for CNN$_2$. The results of the research showed a significant improvement in imaging efficiency and an increase in the sensitivity and accuracy of mapping reference objects. This is especially important in the case of tracking people next to each other and in the case of children. The method is universal and can be used not only in radio tomography but also in other types of tomography, e.g., in electrical, ultrasound, or optical tomography.

Authors: *Grzegorz Kłosowski, Ph.D. Eng., Lublin University of Technology, Nadbystrzycka 38A, Lublin, Poland, E-mail: g.klosowski@pollub.pl; Przemysław Adamkiewicz, Ph.D., University of Economics and Innovation, Projektowa 4, Lublin, Poland, E-mail: przemysław.adamkiewicz@wsei.lublin.pl; Jan Sikora, Prof., University of Economics and Innovation, Projektowa 4, Lublin, Poland, E-mail: jan.sikora@wsei.lublin.pl*

REFERENCES

[1] Styła, M., Adamkiewicz, P., Hybrid navigation system for indoor use. Informatyka, Automatyka, Pomiary W Gospodarce I Ochronie Środowiska, 12 (2022), No. 1, 10-14.
[2] Liu, H.; Darabi, H.; Banerjee, P.; Liu, J. Survey of Wireless Indoor Positioning Techniques and Systems. IEEE Transactions on Systems, Man and Cybernetics Part C: Applications and Reviews, 37 (2007), 1067–1080.
[3] Mishra, A.; Sahoo, U.K.; Maiti, S. Distributed Incremental Strategy for Radio Tomographic Imaging. In Proceedings of the 2020 IEEE 17th India Council International Conference, INDICON 2020; (2020).
[4] Wang, Z.; Zhang, H.; Liu, H.; Zhan, S. Fast Image Reconstruction Algorithm for Radio Tomographic Imaging. Lecture Notes in Electrical Engineering, 236 (2013), 323–331, doi:10.1007/978-1-4614-7010-6_37/FIGURES/6.
[5] Kania K., Rymarczyk T., Mazurek M., Skrzypek-Ahmed S., Guzik M., Oleszczuk P., Optimisation of Technological Processes by Solving Inverse Problem through Block-Wise-Transform-Reduction Method Using Open Architecture Sensor Platform, Energies, 14 (2021), No. 24, 8295.
[6] Cao, X.; Yao, H.; Ge, Y.; Ke, W. A Lightweight Robust Indoor Radio Tomographic Imaging Method in Wireless Sensor Networks. Progress In Electromagnetics Research M, 60 (2017), doi:10.2528/PIERM17052701.
[7] Kłosowski G., Rymarczyk T., Kania K., Świć A., Cieplak T., Maintenance of industrial reactors supported by deep learning driven ultrasound tomography, Eksploatacja i Niezawodnosc – Maintenance and Reliability; 22 (2020), No 1, 138–147.
[8] Koulountzios P., Aghajanian S., Rymarczyk T., Koiranen T., Soleimani M., An Ultrasound Tomography Method for Monitoring CO2 Capture Process Involving Stirring and CaCO3 Precipitation, Sensors, 21 (2021), No. 21, 6995.
[9] Rymarczyk T., Kłosowski G., Hoła A., Hoła J., Sikora J., Tchórzewski P., Skowron Ł., Historical Buildings Dampness Analysis Using Electrical Tomography and Machine Learning Algorithms, Energies, 14 (2021), No. 5, 1307.
[10] Rymarczyk T., Niderla K. Kozłowski E. Król K., Wyrwisz J. Skrzypek-Ahmed S., Gołąbek P., Logistic Regression with Wave Preprocessing to Solve Inverse Problem in Industrial Tomography for Technological Process Control, Energies, 14(2021), No. 23, 8116.
[11] Korzeniewska, E., Sekulska-Nalewajko, J., Gocawski, J., Drożdż, T., Kiebasa, P., Analysis of changes in fruit tissue after the pulsed electric field treatment using optical coherence tomography, EPJ Applied Physics, 91 (2020), No. 3, 30902.
[12] Korzeniewska, E., Krawczyk, A., Mróz, J., Wyszyńska, E., Zawiślak, R., Applications of smart textiles in post-stroke rehabilitation, Sensors (Switzerland), 20 (2020), No. 8, 2370.
[13] Kania, W., Wajman, R., Ckript: a new scripting language for web applications, Informatyka, Automatyka, Pomiary W Gospodarce I Ochronie Środowiska, 12(2022), No. 2, 4-9.
[14] Tan, J.; Guo, X.; Wang, G. Link Selection in Radio Tomographic Imaging with Backprojection Transformation. Lecture Notes in Electrical Engineering (2019), 529, 487–496.
[15] Huang, K.; Tan, S.; Luo, Y.; Guo, X.; Wang, G. Enhanced Radio Tomographic Imaging with Heterogeneous Bayesian Compressive Sensing. Pervasive Mob Comput (2017), 40, 450–463.
[16] Cao, Z.; Wang, Z.; Fei, H.; Guo, X.; Wang, G. Generative Model Based Attenuation Image Recovery for Device-Free Localization with Radio Tomographic Imaging. Pervasive Mob Comput (2020), 66, 101205.
[17] Szczesny, A.; Korzeniewska, E. Selection of the Method for the Earthing Resistance Measurement. Przegląd Elektrotechniczny (2018), 94, 178–181.